The effect of an auxiliary discharge on anode sheath potentials in a transverse discharge

J. E. Foster[a] and A. D. Gallimore[b),c)]
The Plasmadynamics and Electric Propulsion Laboratory, The University of Michigan, Ann Arbor, Michigan 48108

(Received 16 September 1996; accepted for publication 27 December 1996)

A novel scheme that employs the use of an auxiliary discharge has been shown to reduce markedly anode sheath potentials in a transverse discharge. An 8.8 A low-pressure argon discharge in the presence of a transverse magnetic field was used as the plasma source in this study. In such discharges, the transverse flux that is collected by the anode is severely limited due to marked reductions in the transverse diffusion coefficient. Findings of this study indicate that the local electron number density and the transverse flux increase when the auxiliary discharge is operated. Changes in these parameters are reflected in the measured anode sheath voltage. Anode sheath potentials, estimated by using Langmuir probes, were shown to be reduced by over 33% when the auxiliary discharge is operated. These reductions in anode sheath potentials translated into significant reductions in anode power flux as measured using water calorimeter techniques. The reductions in anode power flux also correlate well with changes in the electron transverse flux. Finally, techniques implementing these positive effects in real plasma accelerators are discussed.

I. INTRODUCTION

This work is part of an ongoing investigation whose purpose is to obtain an understanding of the effect that a transverse magnetic field has on anode sheath potentials.[1] The basis of this research is essentially connected to fundamental problems facing designers of various plasma accelerators. More specifically, the plasma accelerators referred to here are used primarily for electric propulsion applications such as satellite station-keeping, orbit transfer, and primary propulsion. This field, known as electric propulsion, is essentially a facet of rocket science that deals with engines which generate thrust by electrical means. These systems are generally categorized into three areas depending on how the thrust is generated:

(1) electrothermal,
(2) electrostatic, and
(3) electromagnetic.

Because a number of these systems utilize nonzero $\mathbf{E}\times\mathbf{B}$ geometries to generate thrust, the need to understand specific plasma–electrode interactions under transverse magnetic field conditions naturally arises. Understanding processes that go on at the electrodes is particularly important in that it yields information on engine lifetime, which is related to erosion phenomena occurring at the electrodes, and on engine efficiency, which is related to energy loss phenomena occurring at the electrodes.

The present research is geared toward understanding the role that the transverse magnetic field plays in driving energy loss processes at the anode. Past studies done on the electromagnetic thruster known as the magnetoplasmadynamic (MPD) thruster have shown that power losses to the anode can be as high as 70% of the input discharge power.[2] Power losses at the anode of MPD thrusters have been shown to be related to the magnitude of the transverse magnetic field component inside the discharge chamber.[3] Ultimately, the goal of this research is to understand why the losses at the anode are so large and to determine how these losses can be significantly reduce through a better understanding of how the near-anode plasma behaves in response to changes in the transverse magnetic field.

This study is primarily a continuation of the near-anode, free burning arc studies conducted at the NASA Lewis Research Center by Soulas and Myers.[3] Their work was essentially a preliminary examination of plasma–anode interactions with the main focus resting upon identifying the effects of the magnetic field (both direction and magnitude) and the local gas pressure on measured anode power flux and on estimated anode fall voltage. The research in this present work, however, concentrates on how changes in plasma properties themselves are related to the formation and growth of the anode fall voltage as a function of transverse magnetic field with the objective being to relate this microscopic viewpoint to the macroscopic one which includes an understanding of anode power deposition in actual MPD thrusters. MPD thruster studies involved in characterizing the changes in the anode fall as a function of operating conditions suggest that ionization phenomena in the near-anode region influence the magnitude of the anode fall voltage.[4,5] It is postulated in this present study that this relationship is associated with the dependence of transverse flux on the local electron number density. Past findings suggest that the ionization rate is a function of the transverse magnetic field.[1] Because of the anode fall voltage's dependence on the local ionization rate and electron number density, the anode fall voltage indirectly becomes a function of the transverse magnetic field. Led by this reasoning, experiments were designed

[a)]Applied Physics Research Assistant.
[b)]Assistant Professor of Aerospace Engineering and Applied Physics.
[c)]Electronic mail: alec.gallimore@umich.edu

 0021-8979/97/81(8)/3422/11/$10.00

to specifically modify charge production in the near-anode region at a fixed magnetic field strength. Of these experiments, the one that was most successful in altering the magnitude of the near-anode electron number density was that which utilized an auxiliary discharge.

The primary aim of this study is essentially threefold:

(1) To determine to what degree that the near-anode plasma can be modified by the use of an auxiliary discharge;
(2) To determine the effect of an auxiliary discharge on measured anode fall voltage and anode power flux; and
(3) To determine possible correlations between changes in the anode fall voltage and anode power deposition with changes in near-anode plasma conditions such as electron number density and transverse flux caused by the operation of the auxiliary discharge.

The effect of the auxiliary discharge on the near-anode plasma is analyzed using a near-anode single Langmuir probe, emission spectroscopy, and water calorimetry.

II. MOTIVATION AND THEORY

As was pointed out earlier, large power losses at the anode of certain classes of plasma accelerators preclude them from serious consideration for near-term space application. A model for the power flux into the anode is given by Cobine:[6]

$$P_a = I_d\left(V_a + \frac{5kT_e}{2e} + \phi_{wf}\right) + P_{c,r}. \tag{1}$$

Here P_a is the energy deposited into the anode per unit time, I_d is the discharge current, V_a is the anode fall voltage (sheath potential drop), T_e is the electron temperature, ϕ_{wf} is the work function of the anode, and finally $P_{c,r}$ is the power contribution due to plasma convection and cathode radiation. Past studies related to **E×B**-type plasma accelerators indicate that the anode fall term is the dominant anode heating source. These findings have been verified by more recent experiments in a transverse discharge diode configuration.[1,3]

Changes in the magnitude of the transverse magnetic field has been shown to have a marked effect on the magnitude and possibly the sign of the anode fall voltage.[1,4] In this study only positive, electron attracting sheath potentials have been observed in the presence of a transverse magnetic field and thus only potentials of this type will be discussed.

In general, the magnitude of the transverse magnetic field controls the transverse flux. Both the transverse diffusion coefficient, $D_\perp$, and the transverse electrical conductivity, $\sigma_\perp$, are reduced when the transverse magnetic field is increased from zero.[7,8] The reduction in the magnitude of these two parameters is on the order of the factor: $1/[1+(\omega_{ce}^2/v_c^2)]$. Here ω_{ce}/v_c, referred to as the Hall parameter, is the ratio of the electron cyclotron frequency to the electron collision frequency. This parameter is a measure of the degree of how ''magnetized'' the electron flow is. For large cyclotron frequencies relative to the collision frequency, electron motion is characterized as a collision driven random walk across magnetic field lines. Clearly, at large transverse magnetic field values, the amount of current that can be supported by the discharge is significantly reduced. Sugwara[9] derived and experimentally tested an expression for the transverse current available in a given plasma for a planar Langmuir probe with a collection surface of area S as a function of transverse magnetic field strength:

$$I_{e\perp} = \frac{1}{4}\cdot e n_0 \overline{v_e} S \cdot \left(\frac{16}{3}\cdot\frac{\lambda_e \alpha^{1/2}}{K(k)\cdot r_0}\right)\cdot\frac{1}{1+\frac{16}{3}\cdot\frac{\lambda_e\alpha^{1/2}}{K(k)\cdot r_0}}. \tag{2}$$

Because Eq. (2) is evaluated at the plasma potential, $I_{e\perp}$ corresponds to the electron saturation or diffusion current available to the anode. Here, λ_e is the electron mean free path, r_0 is the anode radius, n_0 is the electron number density, and $K(k)$ is the elliptic integral of the first kind. The variable α is the ratio of the transverse diffusion coefficient to the diffusion coefficient when the magnetic field is zero and is proportional to the reciprocal of the square of the Hall parameter in the limit of large magnetic field strength. The potential distribution across the anode sheath is determined by the charge distribution in the sheath itself. This charge distribution in turn is controlled by the available flux diffusing into the sheath from the adjacent positive column. In this respect, the magnetic field can control the anode sheath potential difference by controlling the flux in the near-anode region. Experimental results suggest that it is this relationship between the magnetic field and the response (flux and ultimately local electron density) that is responsible for the anode sheath potential variations with the transverse magnetic field.[1]

Again, findings from earlier investigations suggest that the magnitude of electron number density, whose steady-state value is determined by the transverse flux, plays a major role in determining the magnitude of the anode sheath potential difference. Led by these observations, methods to artificially alter near-anode plasma properties at a fixed magnetic field strength were investigated. The most successful method investigated consisted of the operation of an additional, quasi-independent discharge. The main idea behind the concept is based on the fact that an auxiliary electron source could be used to generate additional electron–ion pairs, thus enhancing the conductivity in the both the positive column and the near-anode region in particular. The application of auxiliary discharges to help sustain an otherwise nonsustaining discharge plasma has been used to enhance the performance of CO_2 lasers.[10,11] In certain cases, an electron beam or an auxiliary discharge is used to maintain the proper ionization levels to sustain the discharge while the main discharge electrodes are used to develop an ideal electric field to neutral particle density ratio so as to optimize electron excitation of the laser transition.[10,11] The auxiliary discharge electrons are shared between discharges, benefiting both. The auxiliary discharge essentially plays the role as another energy source that enhances the electron density, which in turn increases the electron flux.

III. EXPERIMENTAL SETUP

The discharge apparatus illustrated in Fig. 1 is mounted in a 1-m-diam. by 1.2-m-long cylindrical vacuum chamber that is evacuated by a rotary gas ballast mechanical pump

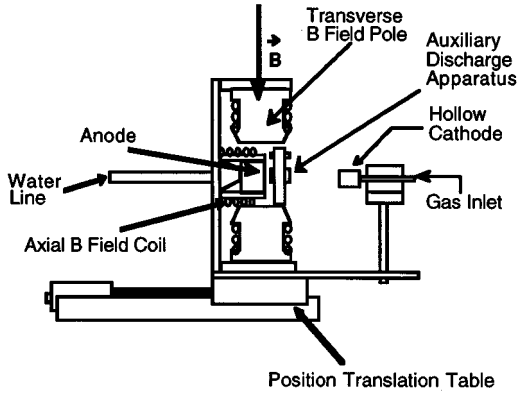

FIG. 1. Experimental apparatus.

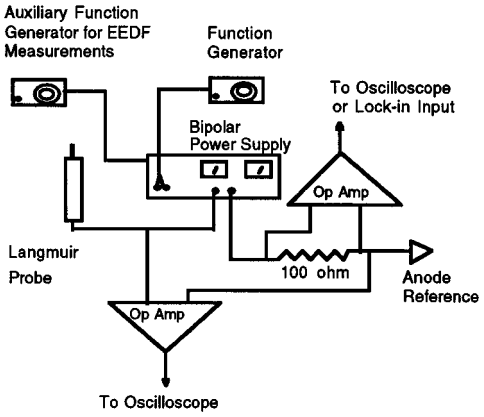

FIG. 2. Langmuir probe circuit.

with a pumping speed of 400 cubic feet per minute. As measured by the chamber thermocouple gauge, once the ultimate pressure of 30 mTorr is reached, the tank is then filled to roughly 1 Torr of argon and flushed several times before the discharge is ignited. Typical operating pressures with the discharge on range between 40 and 50 mTorr.

A gas-fed hollow cathode to the type utilized in many electric propulsion systems is used as the electron source for the discharge. Argon is the working gas for all experiments. The water-cooled stainless steel anode is a 2.5-cm-diam. disk which is thermally and electrically isolated from the electromagnet gantry that it is mounted to. The anode is placed within an alumina sleeve such that its only exposed surface is the front plane facing the cathode. For these experiments, the inter-electrode gap is set to 6.0 cm. The temperature of the anode is monitored via thermocouples attached to the rear of the electrode. The electromagnet, with its shaped pole pieces, immerses the anode and the near-anode region in a uniform magnetic field with the flux lines running parallel to the anode surface. Before the experiment, the magnetic field is measured at the anode surface with a gaussmeter to obtain a calibration curve that is used to correlate electromagnet coil current to the applied field. The region of uniform magnetic field extends to over 3 cm above the surface of the anode.

The discharge is initiated by first pre-heating the hollow cathode and then applying high-voltage between the cathode and a tantalum auxiliary electrode. Once ignited, the arc is transferred to the stainless steel anode and is operated in a constant current mode. After the transfer, the initial attachment at the anode usually consists of a very localized spherical spot at the anode surface. It has been found that a weak transverse magnetic field of $\sim$10 G tends to smear out the spot so that the attachment at the anode is uniform.

For this investigation, an 8.8 A arc is maintained between the cathode and anode. This operating point gives rise to an anode current density of roughly 2 A/cm^2, which is comparable to conditions observed at the anodes of steady-state 100 kW class MPD thrusters.[12]

This study utilizes invasive Langmuir probe techniques and noninvasive emission spectroscopy methods. The Langmuir probe collection surface used in this investigation consists of a 3-mm-long tungsten wire that is 0.2 mm in diameter. The unexposed portion of the tungsten wire is isolated from the discharge via an alumina sheath. The probe is oriented such that its axis is parallel with the magnetic field lines. The probe is located 2.5 mm above the anode surface. The spatial extent of the anode fall region is assumed to be on the order of a Debye length, which for this study was on the order of 10 μm. Thus, the probe was in all cases many Debye lengths from the anode and was not expected to disturb the anode sheath. The probe is connected to a programmable bipolar power supply that is driven by a signal generator so that a triangle wave of a few Hertz is applied to the probe. The measured probe voltage and current are then sent to an operational amplifier which in turn sends the signals to a Tektronix digital oscilloscope. The digital oscilloscope is used to acquire the traces so they can be extracted and stored on a PC via a National Instruments GPIB interface. In addition to standard Langmuir data, electron energy distribution function (EEDF) data are also taken. To make these measurements, an additional signal generator is used to superimpose a 1 kHz, 1 V sine wave on the probe voltage. The probe current signal is then sent to a digital, dual-phase Stanford Research lock-in amplifier which is set to lock in on frequencies at the second harmonic of the 1 kHz superimposed signal. The lock-in amplifier output is then sent to the oscilloscope. The entire setup, including the computer, is plugged into isolation transformers to allow the electrical equipment to float. A block diagram of the Langmuir probe circuit is illustrated in Fig. 2. All Langmuir probe voltage measurements are made with respect to the anode.

The emission spectroscopy setup (Fig. 3) consisted of an iris, a concave/convex doublet, and a Spex 500M 0.5 m spectrometer fitted with a 1800 groove/mm holographic grating. The optics were arranged so the spectrometer collected light from a slice no more than 0.2 mm thick in front of the anode surface. The spectrometer scanned for argon neutral and ion lines located between 470 and 481 nm.

Water calorimetry is used to determine the rate at which energy is deposited into the anode. The cooling water is proved by a Neslab recirculating chiller with a cooling capacity of 950 W. The water flow rate is measured by a standard spring loaded water flow meter. Although the main utility of the water calorimetry resides in the expedition of the

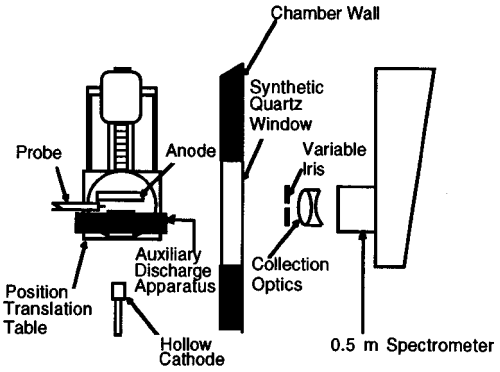

FIG. 3. Emission spectroscopy setup.

heat flux measurements, it also afforded the opportunity to minimize electrode evaporation by removing excess thermal energy. Given the uncertainties in the water flow rate and in the change in water temperature as measured with thermocouples, the measurements associated with this diagnostic possessed an uncertainty which ranged from 15% to 20% depending on operating conditions.

IV. DESCRIPTION OF THE AUXILIARY DISCHARGE APPARATUS AND OPERATION

As mentioned earlier, the purpose of the auxiliary discharge is to modify discharge plasma properties particularly in the near-anode region. The auxiliary discharge apparatus itself is illustrated in Fig. 4. The unit consists of three rectangular molybdenum (Mo) plates 2.8 cm by 4.3 cm and a filament cathode bus all mounted to but electrically and thermally isolated from an aluminum mounting frame. The cathode consists of three oxide-coated, thoriated tungsten wire coils. The oxide paint enhances thermionic emission by lowering the cathode's work function. During operation, electron collection occurs at plate A only (see Fig. 4). As such, electrons emitted from the filament are launched and confined along the magnetic field lines. For this investigation, plates B and C were allowed to float to provide a measure of radial confinement of electrons in the discharge gap enclosed by the auxiliary apparatus. A additional benefit of the arrangement of the plates is the formation of a higher pressure region within the auxiliary region thus enhancing ionization processes there. Also, the floating plates B and C shielded the spectrometer from radiation emitted by the glowing filaments.

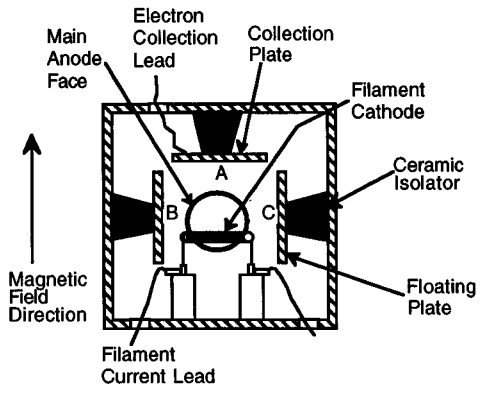

FIG. 4. Auxiliary discharge apparatus.

The auxiliary discharge apparatus was placed downstream of the anode (see Fig. 1) with the Mo collection plate edge lying only 3 mm downstream of the anode. The filaments used in this investigation were operated at emission currents which ranged from 0.0 to 1.3 A. Although the precise mechanisms underlying the enhancement of electron number density in the near-anode region due to the application of an auxiliary discharge are not totally understood, the benefits of the operation of the auxiliary discharge on overall main discharge characteristics, however, are surmised to be associated with:

(1) enhancing of electron bombardment events from an additional electron source;
(2) increasing ionization due to an additional electric field associated with the auxiliary discharge; and
(3) replacing plasma electrons lost to the collection plate by electron emission and production driven by the auxiliary cathode.

This final point is of significance in that the auxiliary anode can collect electrons from the main discharge that would ordinarily diffuse away along the magnetic field. As is the case, the electrons emitted from the cathode can contribute more directly to main discharge processes, acting as a source by both direct emission and charge pair production when the associated auxiliary discharge ionization is taken into account. All in all, the apparatus itself is a tool that provides the means by which discharge plasma properties can be significantly altered. The goal of this investigation is to show that the changes in the main discharge voltage and the anode fall voltage brought on by the auxiliary apparatus are consistent with the expected changes in electron number density and flux.

While operating the auxiliary discharge, the glow from the cathode filaments contributes to the power flux deposited into the anode. In order to account for this, the filament is operated at its nominal heating current of 15 A before the experiment with the discharge off. Power flux due to the filament radiation is then measured. This power is subtracted from the measured anode power flux when the discharge is operating so as to obtain the anode power deposition associated with the discharge only. In addition, this glow has the potential for skewing the intensity profile of collected emission spectra taken by the spectrometer. This effect was found to be fairly small ($<3\%$). The effect of this continuum radiation was reduced for a number of reasons:

(1) the filaments were located between the molybdenum plates and thus were obscured from view of the spectrometer;
(2) the continuum radiation that did scatter into the spectrometer does not change significantly over the wavelength range scanned; and
(3) the peak of the blackbodylike radiation lies far from the wavelength ranges scanned.

V. LANGMUIR PROBE AND EMISSION SPECTROSCOPIC PROCEDURE

Langmuir probe data are acquired as mentioned above by recording collected plasma current as a function of imposed probe voltage. Because the ratio of the probe radius to estimated Debye length exceeds ten, thin sheath analysis applies. The electron number density is obtained from the ion saturation current, i_+, via the relation:

$$i_+ = 0.61 \cdot e \cdot n_e \cdot A_p \cdot \sqrt{\frac{Z_i \cdot kT_e}{M_i}}, \tag{5}$$

where n_e is the electron number density, Z_i is the charge state of the ion species, A_p is the area of the probe, and M_i is the mass of the ion. Because the ion Larmor radius for operating conditions in this experiment is large compared with the probe dimensions, magnetic field effects are not expected to significantly impact density measurements. The error associated with the electron density measurement is roughly 50%.[13] The electron temperature is found by obtaining the slope from the most linear region of a semi-log plot of the electron current versus the probe voltage for those voltage values above the floating potential. The electron temperature is then the reciprocal of this slope if the electron energy distribution is Maxwellian. The plasma potential is obtained by locating the ''knee'' of the semi-log plot. In general, the intersection of the electron retarding region and the electron saturation region is taken to be the ''knee.''[14]

The electron energy distribution function is obtained by using the widely accepted technique of superimposing a small signal onto the probe voltage.[15] A subsequent Taylor expansion of the measured current yields terms which are proportional to the various derivatives of the probe current. The lock-in amplifier detects the second harmonic of the current signal which is proportional to the second derivative of the probe current. Recall that the electron energy distribution function is proportional to the second derivative of the probe current[16]

$$f(E) \propto \sqrt{E} \cdot \frac{d^2 I_p}{dV_p^2}.$$

In the Taylor expansion of the probe current, the second derivative term is proportional to the term containing the second harmonic of the small input ac signal. It is then a simple matter to obtain this second harmonic via a lock-in amplifier. The estimated error in the EEDF measurements is ~8%.[17] Most of the uncertainty in the EEDF measurements is associated with higher order derivatives that contribute to the signal detected by the lock-in amplifier.

Emission spectroscopy measurements were carried out to characterize the near-anode plasma (see Fig. 3). One important aspect of the spectroscopic measurements is that of monitoring the growth or decay of the energetic electron population:

$$\frac{I}{n_e} = \text{const} \cdot \int_{E_r}^{\infty} \sqrt{\frac{2E}{M}} \sigma(E) \cdot f(E) dE. \tag{7}$$

Here the ratio of the intensity, I, of a particular argon line to the local electron number density measured in that region is proportional to the excitation rate for that transition which in turn is proportional to the fraction of those electrons with energies above the excitation threshold for that transition as determined by integrating the electron energy distribution function, $f(E)$. Here $\sigma(E)$ is the excitation cross section as a function of energy, E, and M is the mass of the emitting argon atom or ion.[18] The emission spectroscopy data, therefore, complements the EEDF measurements.

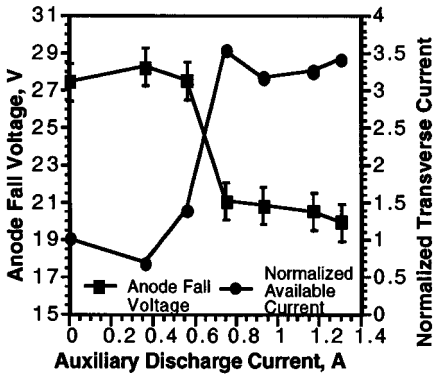

FIG. 5. Anode fall and normalized available transverse current as a function of auxiliary discharge current (38 G).

VI. EXPERIMENTAL RESULTS

One major goal of this study was to artificially modify the electron number density and the transverse flux in the near-anode region and measure the effect of these changes on the anode fall voltage and the anode power deposition. Changes in near-anode plasma properties are measured as a function of filament discharge current at a fixed transverse magnetic field intensity and a fixed main discharge current. In this study, the effect of the auxiliary discharge on a 8.8 A argon discharge was investigated at two representative magnetic field strengths: 38 and 108 G.

A. Correlations between measured anode fall voltage, electron number density, and available transverse current

Figure 5 shows that for the 38 G case, the anode fall was relatively insensitive to changes in the auxiliary current for those currents less than 0.6 A. This behavior is also reflected in the measured electron number density (Fig. 6) and the available transverse current. The available transverse current as calculated using Eq. (2) is normalized to the transverse current available at zero auxiliary discharge current (see Fig. 5). The flatness of the anode fall voltage for these auxiliary currents is interpreted as being directly related to the flatness observed in density and transverse current. Here the plasma conductivity, which should scale with the Hall parameter, is also expected to be constant. In addition, the ratio of the available current to the discharge current inside the anode sheath is also constant. The anode fall voltage should not change under these conditions because excess space charge in the sheath does not vary with the auxiliary discharge current for this current range. For auxiliary discharge currents above 0.6 A, a marked drop in the anode fall voltage is

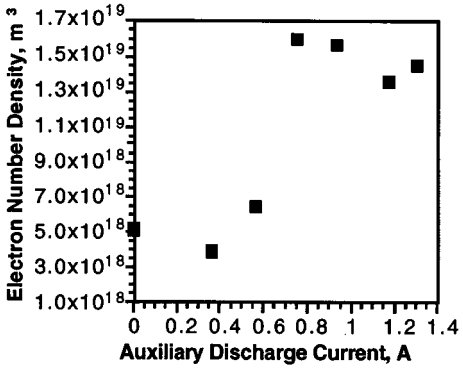

FIG. 6. Near-anode electron density as a function of auxiliary discharge current (38 G).

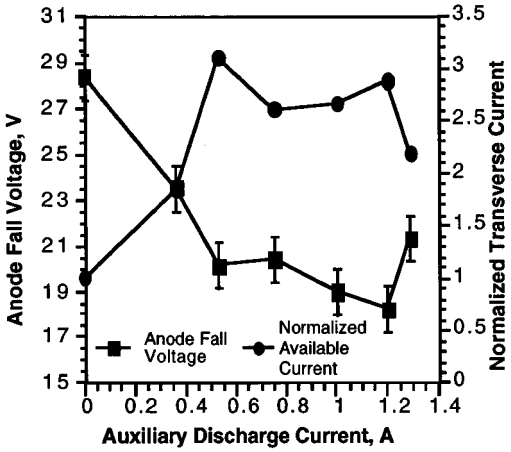

FIG. 8. Anode fall and normalized available transverse current as a function of auxiliary discharge current (108 G).

observed. Also accompanying the change in imposed auxiliary discharge current was a significant jump in electron number density and available transverse current. The ratio of available transverse current to discharge current consequently increases under these fixed magnetic field conditions. At this point, there is an increase in negative space charge in the anode sheath. This uncollected space charge suppresses the potential of the anode relative to the sheath edge, thereby lowering the anode fall voltage. As illustrated in Fig. 7, the relatively large drop in the anode fall voltage and the large jump in the electron number density and calculated available current appear to be related to the significant jump ($\sim$20 V) in the auxiliary discharge voltage required to sustain auxiliary discharge currents greater than 0.6 A. The jump in the auxiliary discharge voltage is postulated to have primarily two effects on the discharge plasma:

(1) Increases in the auxiliary cathode fall voltage enhances ionization along the magnetic field lines because at higher fall voltages the electrons are injected into the positive column at higher energies; and
(2) Increases in the E/p (electric field/gas pressure) ratio along the magnetic field also enhances ionization along the magnetic field.[10]

Subsequent increases in the auxiliary discharge current following the jump did not give rise to any appreciable change in the anode fall voltage. The saturation of the anode fall with increasing auxiliary discharge current is also observed in the electron number density and the available transverse current. This saturation behavior observed in the anode fall voltage is also exhibited in the electron number density and the transverse available current as the auxiliary discharge current increases. As elaborated upon in Sec. II, it is the transverse available current that determines the space charge distribution in the anode sheath, which in turn determines the magnitude of the anode fall voltage. It is no wonder then that the saturation in the anode fall voltage is associated with the saturation of the transverse available current.

Variations in the anode fall voltage with the auxiliary discharge current in the 108 G case (see Fig. 8) behaved similarly to that which was observed in the 38 G case. Initially, however, the anode fall voltage decreases with increasing auxiliary discharge current until the anode fall saturates with increasing values of auxiliary discharge current. The saturation occurred near an auxiliary discharge current of roughly 0.7 A. Variations in the electron number density and available transverse current were consistent with the observed changes in the anode fall voltage. Here, as the density (Fig. 9) and the available current (Fig. 8) increase, the anode

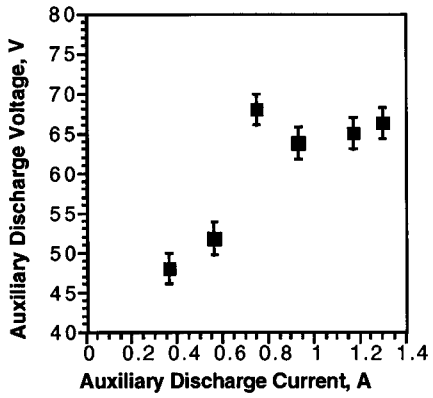

FIG. 7. Auxiliary discharge voltage as a function of auxiliary discharge current (38 G).

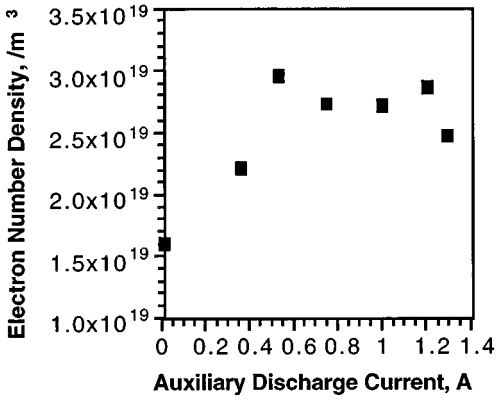

FIG. 9. Near-anode electron density as a function of auxiliary discharge current (108 G).

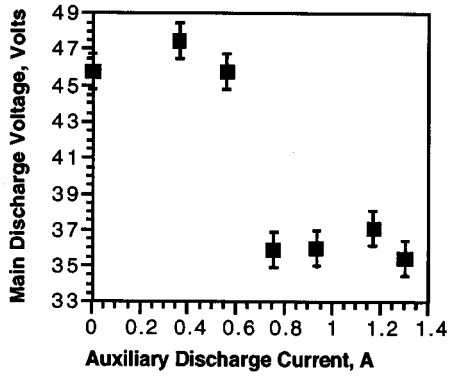

FIG. 10. Main discharge voltage as a function of auxiliary discharge current (38 G).

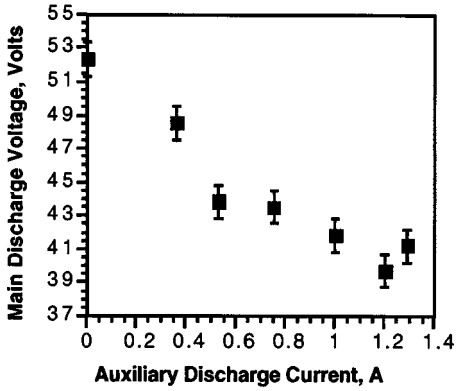

FIG. 11. Main discharge voltage as a function of auxiliary discharge current (108 G).

fall voltage decreases. Saturation in the electron density and available current occur over the same auxiliary current range that the anode fall saturates. Again, this observed behavior is consistent with expected physical processes postulated to occur as the available flux varies.

One primary reason for the saturation in the near-anode electron number density as auxiliary discharge current is varied may be related to electron losses at the auxiliary anode itself. As the auxiliary cathode emission current increases, more plasma electrons in the auxiliary discharge region have to be collected by the auxiliary anode. Under these conditions, in addition to the diffusion-limited environment brought on by the presence of the transverse magnetic field, the auxiliary anode begins to compete with the main discharge for electrons created in this volume as the auxiliary discharge current requirements increase. Saturation in the electron number density is then a consequence of the volume electron/ion production rate balancing losses to the auxiliary anode and the main discharge anode with smaller losses occurring due radial diffusion out of the positive column to the chamber wall and to losses due to volume recombination.

Finally, it should be pointed out that in both the 38 G case and the 108 G case, the auxiliary discharge demonstrates its utility in significantly modifying discharge plasma properties such as density and available flux, which in turn is associated with marked reductions in the anode fall voltage. It is also worth noting that the main discharge voltage in both transverse magnetic field cases followed the same general trends observed in the anode fall (see Figs. 10 and 11). Indeed, the ratio of the anode fall voltage to the discharge voltage was for the most part independent of the auxiliary discharge current. This constancy is associated with the observation that on average the changes in the main discharge voltage can be directly attributed to changes in the anode fall voltage. This behavior suggests that the effect of the auxiliary discharge on the potential distribution across the arc is most pronounced in the anode fall region.

B. Electron energetics: EEDF and emission spectra

The auxiliary discharge has the ability to significantly modify the electron number density and the available transverse flux. Such modifications indicated that the auxiliary discharge must be influencing ionization processes in the near-anode region. Ionization in the volume enclosed by the auxiliary discharge electrodes gives rise to additional ion/electron pairs which diffuse out of this region and flow in the positive column and the near-anode region. EEDF measurements made for this investigation suggest that the energy distribution of the electrons in the near-anode region are not appreciably affected by these processes. Although there is some evidence of EEDF expansion into higher energies, for the most part, as illustrated in Figs. 12 and 13 the curves are fairly insensitive to changes in the auxiliary discharge current. The insensitivity in the electron energy distribution functions as the auxiliary discharge current is varied is consistent with that which is expected from particle and energy balance considerations. In general, the EEDF should be independent of both electron number density and auxiliary discharge power.[19] This insensitivity to changes in the auxiliary discharge current is reflected in the ionization rate per electron (see Fig. 14) calculated by integration of the EEDFs.

The Langmuir probe used to make the EEDF measurements was aligned parallel to the magnetic field so that the energy measurements were sensitive to only those velocity components perpendicular to the surface of the probe. Energy components parallel to the probe's axis, and thus parallel with the magnetic field, cannot be detected by the probe.

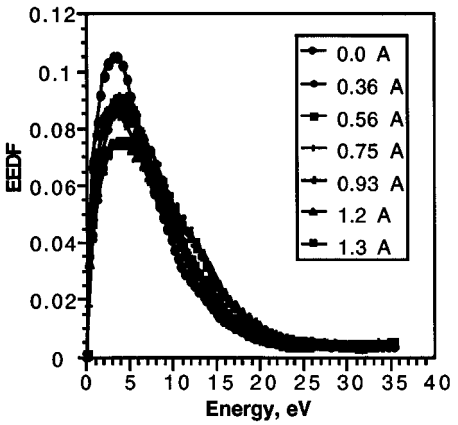

FIG. 12. Variations in the EEDF as a function of auxiliary discharge current (38 G).

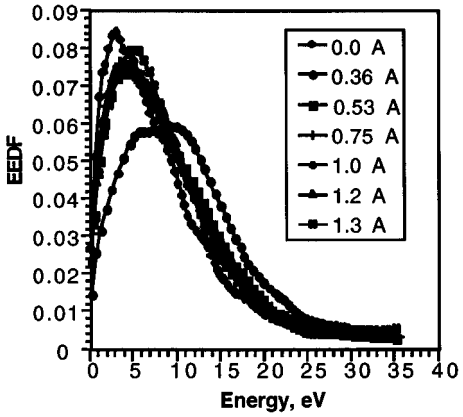

FIG. 13. Variations in the EEDF as a function of auxiliary discharge current (108 G).

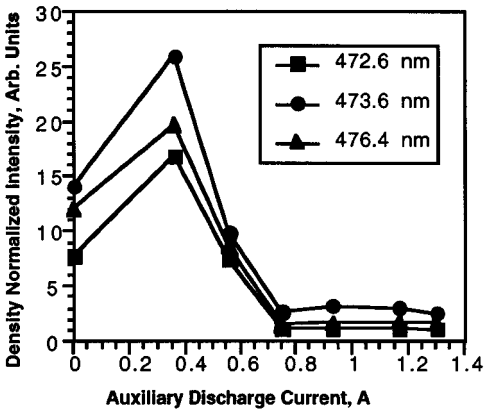

FIG. 15. Variations in near-anode spectra with auxiliary discharge current (38 G).

Because the electric field of the auxiliary discharge is parallel with the magnetic field, such a field can impart energy along this direction to electrons diffusing into this region. In this respect, an energy component associated with the velocities parallel to the magnetic field can be altered, thus possibly increasing the anisotropy of the total EEDF, which would be undetectable by this setup.

Although an investigation into the anisotropy of the resulting EEDF is left to a future study, insight into the behavior of the near-anode electron population as a function of auxiliary discharge current can be obtained by an analysis of the emission spectra. With changes in the auxiliary discharge current, spectral intensity variations of three singly-charged argon ion lines varied in a manner similar to the anode fall and the discharge voltage. In general, when the auxiliary discharge was turned on, the discharge was observed to dim. The ion spectra reveals these trends. A dimming in intensity of the ion lines suggests that either the ion population is decreasing or that the number of electrons capable of exciting the ions is decreasing. In addition, although the subject of a future investigation, the role of variations in the metastable population could also significantly influence the emission intensity as the auxiliary discharge current is varied.

Normalizing the raw intensity data (see Figs. 15 and 16) with respect to the electron density yields a quantity that is proportional to the fraction of electrons with energies greater than the excitation threshold of the line in question. The excitation threshold for the argon ion lines associated with Figs. 15 and 16 is 35 eV.[18] One primary reason for looking at the population of electrons with energies above the 35 eV range was to get a qualitative handle on how the energetic electron population in the distribution tail varied with the auxiliary discharge current. Variations in the population of these electrons provide insight unto the role that superthermal electrons play in ionization processes as auxiliary discharge conditions are varied. These spectra supplement the measured EEDF data. These data suggest that for auxiliary discharge currents of less than 1 A, the fraction of electrons with energies capable of exciting the ion lines decreases with increasing auxiliary discharge current. The observed increases in this parameter at auxiliary discharge currents greater than 1 A for the 108 G case is attributed to similar increases observed in the auxiliary discharge voltage. In addition, the density normalized ion spectra vary roughly as the main discharge voltage varies as a function of auxiliary discharge current, thus suggesting the response of the energetic electrons to variations in main discharge voltage.

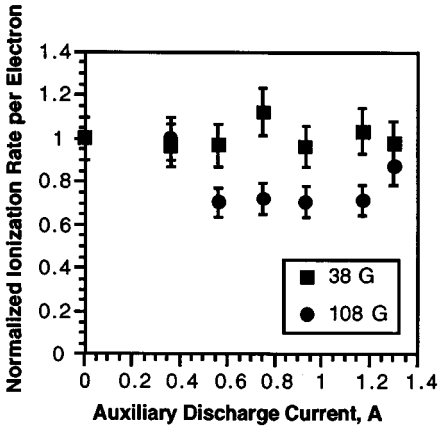

FIG. 14. Near-anode ionization rate as a function of auxiliary discharge current.

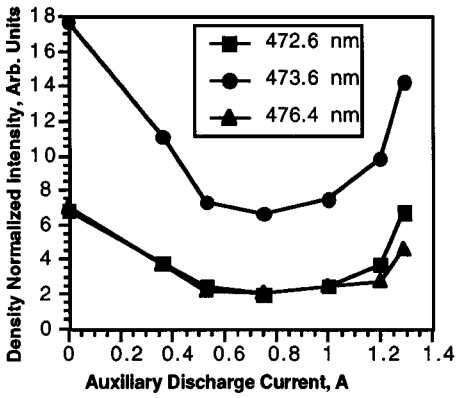

FIG. 16. Variations in near-anode spectra with auxiliary discharge current (108 G).

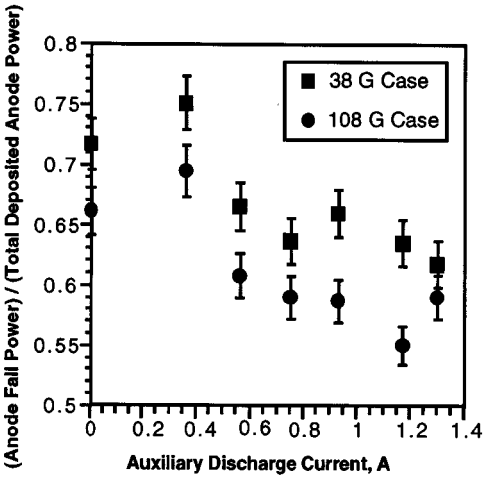

FIG. 17. Variations in anode fall power fractions with auxiliary discharge current.

C. The effect of the auxiliary discharge on anode power deposition

In general, reduction in the measured anode power flux followed measured changes in anode fall voltage as the auxiliary discharge current was varied. Even so, the anode fall power term in Cobine's power flux relation dominated measured anode power deposition (see Fig. 17). However, in both cases the measured trends in the magnitude of power deposited into the anode decreased with increasing auxiliary discharge current. The associated reductions in the anode fall voltage suggest that reductions in the deposited anode power can be as large as 25% in the 108 G case and as large as 15% in the 38 G case (see Fig. 18). If similar reductions in anode power flux could be achieved in MPD thruster systems, efficiencies as high as 55% or better could be realized. At such power levels, the MPD thruster becomes a more realistic propulsion option for energetic space missions.[20]

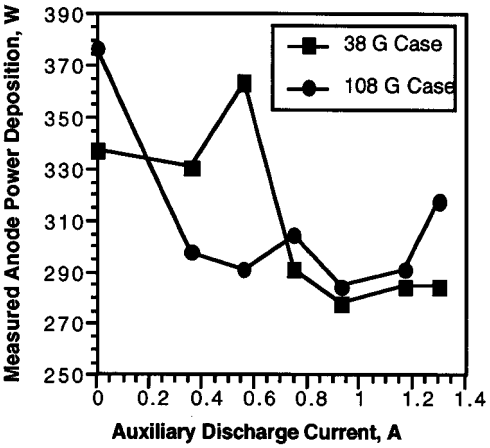

FIG. 18. Variations in measured anode power deposition with auxiliary discharge current (38 G) and (108 G).

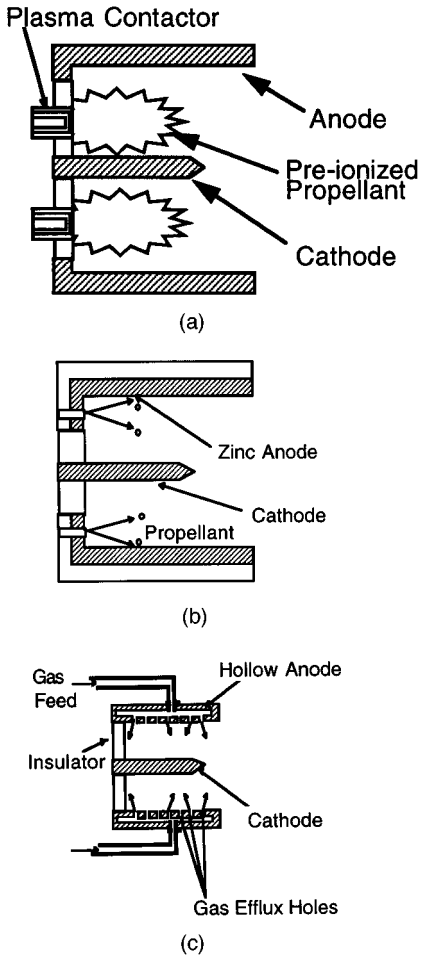

FIG. 19. (a) MPD thruster with propellant pre-ionizers, (b) MPD thruster with zinc anode insert, (c) MPD thruster with hollow anode.

VII. IMPLICATIONS FOR MPD THRUSTERS

Findings from this investigation suggest a possible means for reducing anode fall voltage in MPD thrusters. Throughout this work, it has been emphasized that the electron number density and magnitude of the relative available transverse flux in the near-anode region play key roles in determining the anode fall voltage. In real MPD thrusters the goal is then to increase the relative magnitudes of these parameters at a given thruster operating point. Here, three possible means of achieving these ends are presented and briefly commented upon.

A. Injection of pre-ionized propellant

The injection of pre-ionized propellant into the MPD discharge chamber is perhaps the most direct way to increase the electron density population in the near-anode region. One practical way of accomplishing this is to utilize a plasma contactor as the propellant injector.[21] The plasma contactor, which consists of a hollow cathode enclosed within a coaxial anode, ionizes the propellant that flows through it. As illustrated in Fig. 19(a), this mix of partially ionized gas and neutrals that flows from the orifice of the contactor feeds the main discharge chamber. By varying the plasma contactor discharge current, the ionization fraction of the injected pro-

pellant can be varied. In order to further enhance the coupling of the pre-ionized gas to the near-anode region, the fluid could also be injected in the azimuthal direction or through insulated holes in the anode itself. The only negative aspect of using plasma contactors is associated with the fact that additional power supplies must be utilized to operate the pre-ionizers, thus complicating the hardware simplicity associated with MPD thrusters. The system's complexity, however, may be offset through inherent positives associated with the plasma contactor which include long lifetime and low power consumption.[21]

B. Consumable anode insert

Past researchers have postulated that vaporization of anode material by anode spots can control the behavior of anode power deposition by giving rise to saturation of the anode fall voltage.[5] This observation suggests still another possible means of increasing ionization in the near-anode region. One possible scheme is to utilize an anode made up of an easily ionizable metal such as zinc. This scheme is reminiscent of MPD engines which used metal propellants such as lithium.[22] The liquid metal approach, however, is not attractive due to environmental safety concerns related to the contamination issues and general spacecraft integration questions. If used for essentially primary propulsion, the consumable anode scheme would, however, be essentially immune to most of these concerns, ground-testing notwithstanding. In the consumable anode scheme, as the anode fall increases, the amount of thermal energy that is deposited into the anode also increases. Eventually, the heating of the insert gives rise to evaporation of anode material that is subsequently ionized, thus enhancing the conductivity of the near-anode plasma. This scheme [see Fig. 19(b)] is active in that the amount of metal vapor from the anode that enters into the plasma depends on the magnitude of the anode fall. In steady-state, the anode fall should saturate because increases in anode fall give rise to increases in metal vapor, which in turn should bring the anode fall down to a steady-state value. By carefully selecting the insert anode material, a limit on the largest anode fall that will develop can be established. A secondary concern associated with this concept involves the lifetime of the anode. It is conceivable, however, that a consumable anode of sufficient thickness and hence lifetime can be successfully utilized to control the anode life problem.

C. Increasing discharge chamber pressure

A ''free burning'' arc study conducted by Soulas and Myers[3] showed that increasing the local pressure decreases the anode fall voltage at a fixed transverse magnetic field strength. In addition, an MPD thruster study conducted by Myers[20] indicated that thruster anode radius and flow rate affect the anode fall voltage. The anode fall voltage was found to drop with increasing propellant flow rate and reduced discharge chamber radius. In general, decreasing the anode radius and/or increasing the propellant mass flow rate increases the discharge chamber pressure. These studies suggest yet another means for increasing ionization in the near-anode region. Because the density of neutrals increases with increasing pressure, the ionization probability for a given electron increases as well. As density increases, so must the available transverse flux. In order to enhance ionization phenomena in the near-anode region, propellant injection through efflux holes in the anode itself may be implemented. This hollow anode scheme, illustrated in Fig. 19(c), would allow for a higher local neutral density in the near-anode region, thus increasing the likelihood of increased ionization occurring there.

VIII. SUMMARY

Significant modifications to the near-anode plasma of a transverse discharge were demonstrated through the application of an auxiliary discharge. Marked increases in the electron number density and available transverse flux brought on by the use of the auxiliary discharge gave rise to moderate reductions in the anode fall voltage. The main discharge voltage behavior was similar to the anode fall as the auxiliary discharge current was varied. The measured electron energy distribution functions were found to be insensitive to the changes in the auxiliary discharge current. This finding suggests that from an energy standpoint, the bulk electron population was not appreciably affected by the operation of the auxiliary discharge. However, possible anisotropy in the EEDF due to electric fields or an electron beam component associated with the auxiliary discharge could play an important role in determining overall ionization rates. Because the anode fall voltage dominates anode power deposition in this transverse discharge, decreases in the anode fall voltage gave rise to reductions in the measured anode power deposition by as much as 25%. If such reductions in anode power flux could be made in MPD thrusters, these devices would then make a more realistic candidate for energetic space missions. The effect of an auxiliary discharge can possibly be achieved in MPD engines by utilizing components which enhance the near-anode electron number density. Such systems changes range from the use of pre-ionizers to increasing the pressure in the near-anode region of the discharge chamber. All of these possible techniques must be economical, clean, and robust in order to minimize spacecraft integration issues.

ACKNOWLEDGMENTS

The authors would like to thank the National Aeronautics and Space Administration Lewis Research Center, Low Thrust Propulsion Group, as well as the National Physical Science Consortium Fellowship Program which helped facilitate this research.

[1] J. E. Foster and A. D. Gallimore, Phys. Plasmas **3**, 4239 (1996).
[2] R. Myers, NASA Contractor Report 187163, AIAA-91-2342 (1991).
[3] G. Soulas and R. Myers, *Proceedings of the 23rd International Electric Propulsion Conference* (The Electric Rocket Society, Columbus, OH, 1993), IEPC 93-194.
[4] H. Hugel, IEEE Trans. Plasma Sci. **PS-8**, 437 (1980).
[5] K. D. Diamant, E. Y. Choueiri, and R. G. Jahn, *Proceedings of the 25th International Electric Propulsion Conference* (The Electric Rocket Society, Columbus, OH, 1995), IEPC 95-234.
[6] J. Cobine and E. Burger, J. Appl. Phys. **26**, 895 (1955).
[7] F. Chen, *Introduction to Plasma Physics and Controllable Fusion* (Plenum, New York, 1984), Chap. 5, Sect. 5.10.

[8] H. Kaufman, *Operation of Broad Beam Ion Sources* (Commonwealth Scientific Corporation, VA, 1984), Chap. 15, Sect. G.
[9] M. Sugawara, Phys. Fluids **9**, 497 (1966).
[10] Y. P. Raizer, *Gas Discharge Physics* (Springer, New York, 1991), Chap. 4, Sect. 4.1, Chap 14, Sect. 14.3.4.
[11] R. E. Beverly III, *Proceedings of the SPIE 7th International Symposium on Gas Flow and Chemical Lasers* (SPIE, Bellingham, 1988), Vol. 1031.
[12] A. D. Gallimore, A. Kelly, and R. Jahn, AIAA J. **9**, 361 (1993).
[13] D. Tilley, A. Kelly, and R. Jahn, *Proceedings of the 21st International Conference on Electric Propulsion* (American Institute of Aeronautics and Astronautics, Washington D.C., 1990), AIAA 90-2667.
[14] J. Swift and M. Schwar, *Electrical Probes for Plasma Diagnostics* (Lliffe Books, New York, 1970), Chap. 1, Sect. 1.5, Chap. 12, Sect. 12.6.
[15] H. Rundle, D. Clark, and J. Dechers, Can. J. Phys. **51**, 144 (1973).
[16] M. Druyvesteyn, Z. Phys. **24**, 781 (1930).
[17] J. E. Heidenreich III and J. R. Paraszczak, J. Vac. Sci. Technol. B **6**, 286 (1980).
[18] T. L. Cox, V. G. I. Deshmukh, D. A. O. Hope, A. J. Hydes, N. St. J. Braithwaite, and N. M. P. Benjamin, J. Phys. D **20**, 820 (1987).
[19] M. A. Lieberman and A. J. Lichtenberg, *Principles of Plasma Discharges and Materials Processing* (Wiley, New York, 1994), Chap. 10, Sect. 10.2.
[20] R. M. Myers, M. Mantenieks, and J. Sovey, *Proceedings of the 21st International Electric Propulsion Conference* (American Institute of Aeronautics and Astronautics Publishing, Washington D.C., 1990), AIAA 90-2669.
[21] G. C. Soulas, *Proceedings of the 30th AIAA Joint Propulsion Conference*, (American Institute of Aeronautics and Astronautics Publishing, Washington D.C., 1994), AIAA 94-3310.
[22] D. B. Fradkin, Ph.D. thesis, Princeton Aerospace and Mechanical Science Department, 1973.